Computers in Biology and Medicine 200 (2026) 111371

Contents lists available at ScienceDirect

Computers in Biology and Medicine

journal homepage: www.elsevier.com/locate/compbiomed

Bayesian parameter inference and uncertainty-informed sensitivity analysis in a 0D cardiovascular model for intraoperative hypotension

Jan-Niklas Thiel [a,*], Marko Zlicar [b], Ulrich Steinseifer [a], Borut Kirn [c,1], Michael Neidlin [a,1]

[a] Cardiovascular Engineering, Applied Medical Engineering, Medical Faculty, RWTH Aachen University, Aachen, Germany
[b] Clinical Department of Anaesthesiology and Intensive Therapy, University Medical Centre Ljubljana, Ljubljana, Slovenia
[c] Institute of Physiology, Medical Faculty, University of Ljubljana, Ljubljana, Slovenia

ARTICLE INFO

Keywords:
Lumped parameter modeling
Cardiovascular modeling
Reduced-order modeling
Bayesian parameter inference
Uncertainty quantification
Global sensitivity analysis

ABSTRACT

Computational cardiovascular models are promising tools for clinical decision support, particularly in complex conditions, such as intraoperative hypotension (IOH). IOH arises from different mechanisms, making treatment selection non-trivial. Patient-specific predictions require calibration, typically performed using classical optimization prone to parameter non-identifiability and lacking uncertainty quantification, hindering clinical translation. Consequently, Bayesian approaches are needed that facilitate parameter inference, sensitivity analysis, and uncertainty quantification in cardiovascular models.

We utilize Bayesian Markov chain Monte Carlo (MCMC) to estimate parameter distributions of a cardiovascular lumped parameter model (LPM) across different IOH scenarios. We demonstrate parameter non-uniqueness and its impact on sensitivity indices. We improve parameter reliability by incorporating clinical knowledge and measurement uncertainties. Continual learning of the model is achieved by sequential parameter updating as new patient data become available. We introduce an uncertainty-aware sensitivity analysis and compare it with a classical approach.

Classical optimization yielded many local solutions for IOH, with notably different sensitivities. MCMC distinguished different hypotension scenarios, such as those induced by impaired contractility or hypovolemia. Parameter uncertainty decreased by about 70 % with additional data, and by up to 94 % with sequential updating. Propagating uncertainties from MCMC through sensitivity analysis provided tighter credible intervals, resulting in more stable parameter rankings than the classical approach. The Bayesian approach revealed differences in model sensitivity and treatment suggestions across patient conditions, highlighting the potential to inform therapy planning.

Combining Bayesian inference with sequential updating and sensitivity analysis improves the reliability and identifiability of parameter estimates, enhancing the clinical utility of LPMs for therapy guidance.

1. Introduction

Computer models offer the potential to support clinical decision-making in complex, highly patient-specific settings. One example is the treatment of intraoperative hypotension (IOH). IOH is characterized by a significant decrease in mean arterial pressure (*MAP*) and may be caused by various factors, including severe vasodilation (vasoplegia), hypovolemia due to blood loss, or reduced ventricular contractility [1,2]. Much research has focused on developing algorithms to predict IOH. Work from Hatib et al. [3] has developed one such algorithm, the Hypotension Prediction Index (HPI), that is already applied in clinical practice [4–6]. The HPI predicts the risk of IOH occurring within the next 10 min using a score ranging from 0 to 100. However, it does not directly support clinical decision-making regarding the best intervention strategy once IOH occurs in these patients. This is crucial because it is often difficult to know a priori which option will effectively treat the underlying cause and increase the *MAP* to a safe level [7–12]. Treatment options include vasopressors to induce vasoconstriction, inotropes, used to increase cardiac contractility, and intravenous fluid boluses to increase overall systemic pressure. Therefore, it is desirable to provide clinical decision support that estimates the effect of each treatment option for individual patients with IOH. Computational models can

* Corresponding author. Institute of Applied Medical Engineering, Forckenbeckstr. 55, 52074, Aachen, Germany.
E-mail address: thiel@ame.rwth-aachen.de (J.-N. Thiel).
[1] These authors contributed equally to this work.

https://doi.org/10.1016/j.compbiomed.2025.111371
Received 19 September 2025; Received in revised form 11 November 2025; Accepted 1 December 2025
Available online 6 December 2025
0010-4825/© 2025 The Authors. Published by Elsevier Ltd. This is an open access article under the CC BY license (http://creativecommons.org/licenses/by/4.0/).

deliver this information [13].

Any computational tool intended for clinical use must be efficient and robust and require minimal user input to reduce misuse and inter-operator variability. Lumped parameter models (LPMs) meet these requirements and have been applied to various biological systems, for example, the human cardiovascular system [14–17]. These models divide the human body into an arbitrary number of 0D compartments represented by Windkessel elements of different orders. This results in a set of ordinary differential equations and unknown model parameters, which can vary in magnitude depending on the patient and pathology. The advantage of LPMs is that they are derived from physiological mechanisms, making their parameters clinically interpretable. However, calibrating complex, multi-parameter LPMs is often challenging as highly nonlinear relationships between model parameters and outputs can lead to parameter non-identifiability, resulting in non-unique solutions [18–20]. In practice, calibration is typically performed using optimization-based point estimation, which provides a single parameter vector, but does not quantify associated uncertainties in the estimates [21–24]. Both parameter identifiability and uncertainty quantification (UQ) are crucial for robust clinical decision-support systems because multiple, physiologically distinct parameter combinations can reproduce the same clinical measurement, leading to different model behavior and unreliable predictions. This fundamental problem can be addressed in various ways. One approach is to rank parameters and reduce the number of free parameters included in the calibration using a sensitivity analysis, while retaining the overall model structure [25]. As an alternative approach, uncertainties can be explicitly considered in the calibration (inverse UQ), and the resulting predictions and credible intervals must lie within clinically meaningful thresholds for the model's intended context of use. The model can be considered sufficiently calibrated if the uncertainty of the task-specific prediction - which may refer to specific treatment indications or risks, or be used for diagnosis and disease classification - lies within the defined limits [26].

Unlike classical optimization approaches that yield deterministic point estimates, Bayesian inference provides statistical distributions, called posterior distributions, of parameter values that have the highest likelihood of producing certain observed data. It enables the quantification of various sources of uncertainty in the measurement data and their propagation to model outputs by sampling from the estimated posterior distributions and performing forward simulations. A sampler iteratively updates user-defined prior distributions to obtain those posteriors. These priors can contain different amounts of information and can be defined based on previous experiments or clinical (expert) knowledge. When little to no information is available, they can be weakly or non-informative [27]. For instance, priors can be defined as a uniform distribution within known physiological ranges or as a normal distribution considering a specific diagnosis. For instance, if a patient presents with reduced cardiac function, a higher likelihood of decreased ventricular contractility can be assumed. Posterior distributions can also be updated sequentially as new measurement data become available by using posteriors from a previous time instance as new priors. This follows the concept of recursive Bayesian estimation, which is thoroughly described by Särkkä et al. [28], and coupled with the Markov chain Monte Carlo (MCMC) method by Hooten et al. [29] and Agand et al. [30]. This avoids having to recalibrate a Bayesian model from scratch, which saves computational resources and time [31,32]. It also allows the effect of time on parameters to be included in an on-line learning fashion [28]. MCMC has been used in several studies, including those related to cardiovascular LPMs [26,33–36]. A practical limitation of Bayesian approaches is that they require a large number of model evaluations for parameter inference, which can be computationally infeasible for large, complex models, particularly in clinical practice. Consequently, reduced order models (ROMs) are often used to accelerate sampling [36,37].

The problem of parameter identifiability can be addressed by conducting a sensitivity analysis with subsequent reduction of free parameters. This involves varying the model parameters within defined ranges and quantifying their effect on the model outputs. The most prominent approach is the Sobol method, a variance-based global sensitivity analysis (GSA) [38–40]. The resulting sensitivity indices can be used to rank the parameters and define subsets for the calibration process that exclude correlated parameters [25,41–43]. To ensure a robust calibration procedure for all patients and pathologies, these rankings must be valid across the entire output range of interest (e.g., patients with normotension, hypotension, and hypertension). In this context, determining plausible ranges of input parameter distributions is often challenging and depends on the model's context of use. Ideally, these ranges are chosen based on prior literature and domain knowledge. However, many studies conduct a GSA at a single, fixed model state, and perturb the nominal parameter set only within small ranges [23,44–47]. When information on parameter bounds is unavailable, filtering methods such as Bayesian history matching or Monte Carlo filtering provide a more reliable way to restrict parameter values to ranges that reproduce expected physiological outputs. These methods can also identify dependencies between parameters, which can be incorporated into sampling for GSA or model calibration [48,49].

Besides reducing free parameters for model calibration, GSA could also support clinical decision-making by linking most sensitive parameters to their physiological mechanisms and corresponding treatments. Essentially, a GSA could improve the understanding of how the human body responds dynamically to specific therapies and medications. In this context, their effects can be represented by small, local perturbations around a nominal parameter set that reproduces some patient data, rather than conducting a GSA on the entire feasible range of the model parameters. When the model exhibits non-identifiability, meaning multiple parameter sets predict a patient's clinical data equally well, then the sensitivity indices used for therapy suggestions may vary across these parameterizations. To obtain reliable therapy suggestions, the uncertainty in patient-specific nominal parameter sets should be propagated through the GSA to generate distributions (with confidence/credible intervals) for the Sobol indices [42,50–52]. This can be achieved through upstream Bayesian inference and repeated GSAs with draws from the posterior parameter distributions and corresponding parameter perturbations induced by a certain therapy or medication. To the author's knowledge, no study with a clinical focus has yet considered uncertainties in sensitivity indices. This idea is similar to the approach used by Eriksson et al. to analyze dynamical intracellular pathway models [49].

One clinical pathophysiological event that would benefit from supporting therapy decisions with sensitivity indices is IOH. There is non-uniqueness in interventions (vasopressors, inotropes, and fluid boluses) that can potentially lead to the same desired clinical outcome (an increase in *MAP*). Because parameters of cardiovascular LPMs (resistances, compliances, elastances) have clear physiological meanings, they can be mapped to the available treatments for IOH. We hypothesize that, for a given patient, the parameters with the highest sensitivity can identify the most promising treatment option for hemodynamic resuscitation.

First, this study aims to highlight the effect of parameter non-uniqueness on sensitivities derived from GSA, which can be particularly problematic for deterministic point estimates from classical optimization approaches. Second, the study aims to develop a methodology to integrate UQ into GSA to produce uncertainty-aware sensitivity indices with credible intervals. Third, it aims to evaluate the reliability of suggestions derived from these two approaches in the context of clinical decision-support. This contribution promotes the translation of computational models as tools for prediction and therapy guidance. For this purpose, we use a cardiovascular LPM to model the clinical scenario of IOH. In the classical approach, we identify all parameter combinations that yield the same IOH output (mimicking deterministic point estimates from classical optimization approaches) and perform a GSA for each. In the uncertainty-aware approach, we train a ROM and perform Bayesian inference using MCMC to obtain posterior

distributions that reproduce the event of IOH. These posteriors are then propagated through GSA to obtain distributions and credible intervals of the sensitivity indices.

2. Materials and methods

2.1. Model structure and classical parameter estimation

An LPM of the cardiovascular system was taken from previous work. The model consists of 12 compartments describing the hemodynamics of the heart and the systemic and pulmonary circulation, as shown in Fig. 1. Cardiac function is modeled using an elastance-driven pressure-volume relationship, and vessels are represented by resistance, compliance, and inertance elements. More detailed information about its implementation and all parameter values used can be found in the Appendix and in previous work [53]. Model inputs are the systolic elastance of the left ventricle *Emaxlv*, the resistance of the systemic microcirculation *Rmc*, the change in the patient's total blood volume *TBV*, and the heart rate *bpm*. The model computes pressures and flows and reported outputs are cardiac output *CO*, mean arterial pressure *MAP*, and pulse pressure *PP*. The healthy baseline represents a 36-year-old female patient (164 cm, 56 kg). This synthetic case has a total blood volume of 3900 mL, and a total stressed blood volume of approximately 550 mL.

The simulation time was set to 100 s, with an adaptive time step of 5×10^{-4} s and the ODE system was solved using the Dormand Prince algorithm. The last two cycles were evaluated. There are three therapy options for IOH. The first is inotropes, which increase ventricular contractility and may elevate both *CO* and *MAP*. In contrast, vasopressors increase systemic vascular resistance through vessel constriction, which tends to decrease *CO* while increasing *MAP*. Administering an additional fluid bolus elevates *MAP* and can affect *CO* differently depending on whether vasoplegia is present (*CO* increases) or cardiac function is impaired (*CO* decreases). These treatment options were linked to specific model parameters. The effect of inotropes was mimicked by increasing the systolic elastance of the left ventricle *Emaxlv*. Vessel constriction due to vasopressors was represented by increasing the resistance of the systemic microcirculation *Rmc*, the largest compartment of the arterial system. Because additional fluid increases intravascular pressure, this effect was modeled by adding a pressure source term to the differential equation of the systemic venous compartment (*svn*, see Fig. 1). Instantaneous infusion or loss of fluid induces a pressure change *dPinf*, implemented by relating the change in the patient's total blood volume *TBV* to the compliance of the systemic venous compartment *Csvn* and a pulse duration t_{inf}. This source term is applied once the simulation reaches a stationary state:

$$dPsvn = dPsvn + dPinf, \tag{1}$$

$$dPinf = \frac{TBV}{Csvn^{*}t_{inf}}. \tag{2}$$

The pulse duration t_{inf} is set to 0.01 s. Ramping up and down is implemented using a smoothed Heaviside function to avoid discontinuities, which improves adaptive time-stepping and the stability of the gradient calculation.

To illustrate the issue of non-uniqueness in classical optimization approaches that yield deterministic point estimates, the LPM was evaluated at varying values of *Emaxlv*, *Rmc*, and *TBV* within physiologically admissible ranges, as presented in Table 1 and derived from the literature. Grid sampling was used to generate 343 samples. The results for non-sampling points were determined using cubic spline interpolation. Results for *MAP* and *CO* were then visualized using heatmaps, with one parameter fixed to its median value at a time. Additionally, contour lines were created for hypotension reference thresholds of *MAP* = 65 mmHg

Table 1
List of the input and output parameters of the model. Input ranges denote physiologically admissible ranges of the model, which are used for the analysis of the classical and Bayesian approaches.

Parameter	Range	Type	Reference
Systolic elastance of the left ventricle *Emaxlv* in mmHg mL^{-1}	[0.1, 5.0]	Input	[22,24]
Resistance of the systemic microcirculation *Rmc* in mmHg s mL^{-1}	[0.1, 2.0]	Input	[22,24]
Change in total blood volume *TBV* in mL	[-500, 500]	Input	[54]
Heart rate *bpm* in min^{-1}	[50, 120]	Input	
Cardiac output *CO* in L min^{-1}	–	Output	
Mean arterial pressure *MAP* in mmHg	–	Output	
Pulse pressure *PP* in mmHg	–	Output	

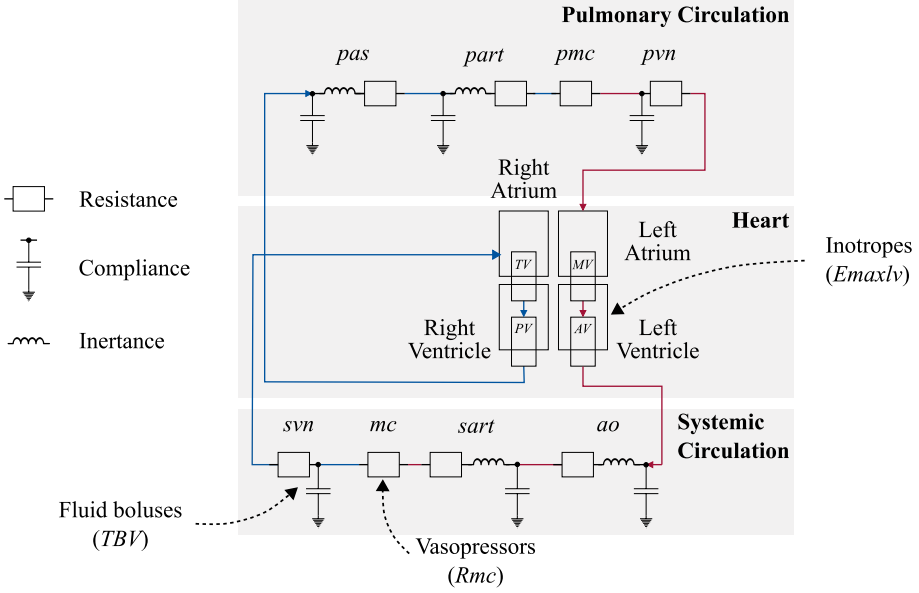

Fig. 1. Overview of the cardiovascular lumped parameter model, taken from previous work [53]. Linked changes representing different treatments for intraoperative hypotension are shown with dashed arrows.

and $CO = 3$ L min^{-1}, as well as for 10 % deviations from these values (giving a reference region).

2.2. Global sensitivity analysis

A variance-based GSA was utilized to quantify the effects of changes in the input parameters *Emaxlv*, *Rmc* and *TBV*, which are proxies for the treatment of IOH, on the model outputs *MAP* and *CO*. Total order sensitivities were computed using the Sobol method, yielding indices ranging from zero to one. Higher values indicate a greater influence of the corresponding model parameter on the clinical marker. In general, first order indices can measure the effect of changing a single parameter alone, representing its main effect on each model output. The total order sensitivity indices, on the other hand, can quantify variances caused by interactions with other input variables. They can be calculated using the formula given by Homma and Saltelli [39]:

$$S_{T,i} = 1 - \frac{\mathrm{Var}_{x_{\sim i}}\left(E_{x_i}(y|x_{\sim i})\right)}{\mathrm{Var}(y)} = \frac{E_{x_{\sim i}}\left(\mathrm{Var}_{x_i}(y|x_{\sim i})\right)}{\mathrm{Var}(y)}. \quad (3)$$

Here, y denotes the scalar model output and x_i is the ith model input. $x_{\sim i}$ refers to all model inputs except x_i. $\mathrm{Var}(y)$ is the total, unconditional variance of the output y. $E_{x_{\sim i}}\left(\mathrm{Var}_{x_i}(y|x_{\sim i})\right)$ is the expectation over $x_{\sim i}$ of the conditional variance $\mathrm{Var}_{x_i}(y|x_{\sim i})$ with respect to x_i. This represents the portion of $\mathrm{Var}(y)$ attributed to x_i, including all interactions. The Sobol method was implemented using the *SALib* package and more details can be found in previous work [53,55].

A GSA was conducted for each of the 343 nominal parameter sets sampled from the ranges listed in Table 1. For each nominal parameter set, the ranges of *Emaxlv*, *Rmc*, and *TBV* were derived by applying perturbations that mimic the changes induced by each clinical treatment option. The magnitude of each perturbation was derived from the literature and is listed in Table 2. All other model parameters were kept constant. Saltelli's extension of the Sobol' sequence was used for sampling with a sample size of $N = 512$ and $D = 3$ cardiovascular system parameters. This resulted in $N(2D+2) = 4,096$ model evaluations, for which *MAP* and *CO* were computed. Total order sensitivity indices S_T were calculated using these input and output pairs.

By performing a GSA on each sample point derived from the ranges listed in Table 1, the sensitivity of the model could be quantified across the entire input parameter space. The sensitivities of each parameter were illustrated using heatmaps, in which the colors are weighted by each parameter's individual contribution to the sum of S_T. This provides insight into which parameter is most sensitive to *MAP* and *CO* at any given point in the parameter space.

2.3. Bayesian parameter inference

Since Bayesian inference with MCMC requires a large number of model evaluations, we trained ROMs to make model calibration efficient and computationally feasible for clinical application. These substitutes for the full order cardiovascular LPM follow:

$$(CO, MAP, PP) = g(Emaxlv, Rmc, TBV, bpm; \beta). \quad (4)$$

As previously described, model inputs are *Emaxlv*, *Rmc*, *TBV*, and *bpm*, while model outputs consist of *CO*, *MAP*, and *PP*. $\beta_i \in \mathbb{R}$ are model parameters specific to the trained ROM. The open-source Python tool *SASQUATCH*, which was developed in a previous study, was used to train Non-Intrusive Polynomial Chaos Expansion (NIPCE) models of different orders. In this context, $\beta_i \in \mathbb{R}$ are the estimated expansion coefficients for each polynomial basis term. Cheng et al. and our previous study provide more details on the formulation and theoretical background of NIPCE models [55,61]. 5000 data points were generated by sampling from the ranges presented in Table 1 using Latin hypercube sampling and by evaluating the cardiovascular LPM for these samples. Training and testing were performed using k-fold cross-validation with ten equally sized random splits. The performance of the models was compared using the R^2 score and the mean absolute percentage error (*MAPE*), shown in Figure S-1 in the Appendix. For the following analysis, we used the NIPCE model of order three.

MCMC is a collection of algorithms used to produce dependent samples that approximate the joint distribution of model parameters for a computational model describing patient-specific or clinical cohort data, while accounting for uncertainty. They create Markov chains that start from arbitrary parameter values, which, after an initial burn-in, eventually converge to a target posterior distribution. Prior distributions, which reflect initial beliefs and incorporate clinical knowledge, are combined with a likelihood, which links the model to measurement data and accounts for uncertainties, such as noise, outliers, and other measurement errors. Combining both, these define the posterior (i.e., the updated belief), which is the target distribution that MCMC aims to sample from. Common algorithms include Metropolis-Hastings, Gibbs sampling, slice sampling, and Hamiltonian Monte Carlo (HMC), including the No-U-Turn Sampler (NUTS). These algorithms iteratively draw many dependent samples and produce chains that explore the parameter space, attempting to move to points that are more probable than the existing ones, i.e., points in higher-density regions. Samples obtained from the initial burn-in phase are discarded. The retained draws provide distributions for each parameter, rather than single-point estimates (as in classical optimization), from which one can report means, medians, and credible intervals. Accounting for uncertainties contributes to enhancing the reliability of parameter estimates and subsequent model predictions, a critical aspect for clinical translation. A more thorough description of the theory and concepts behind MCMC can be found in the comprehensive works of Speagle [27], van de Schoot [62] et al., and Hartig et al. [63].

The cardiovascular model parameters *Emaxlv* and *Rmc* were estimated by using the MCMC implementation of the open-source Python package *PyMC*. For outputs $O = \{CO, MAP, PP\}$ and observations $y_{o,i}$ with $o \in O$ and $i = 1, \ldots, N$, the likelihood function was defined using a univariate normal distribution

$$p(y|X, \theta, \beta) = \prod_{o \in O} \prod_{i=1}^{N} \frac{1}{\sqrt{2\pi}\,\sigma_o} \exp\left(- \frac{\left[y_{o,i} - g_o(\theta, TBV_i, bpm_i; \beta)\right]^2}{2\sigma_o^2} \right). \quad (5)$$

Here, $\theta = (Emaxlv, Rmc)$ are the unknown model parameters to be inferred and $X = \{TBV_i, bpm_i\}_{i=1}^{N}$ are observed inputs. For each output o, σ_o is the defined measurement standard deviation and g_o denotes the corresponding ROM prediction. Based on how synthetic measurements were created, independence across outputs and observation indices can be assumed. This implies a diagonal covariance $\sum = diag(\sigma_{CO}^2 I_N, \sigma_{MAP}^2 I_N, \sigma_{PP}^2 I_N)$. The gradient-based NUTS algorithm was utilized and the change in total blood volume (*TBV*) and the heart rate (*bpm*) were treated as clinically measurable inputs and kept fixed. Four chains were run, each using 5000 samples after an initial burn-in of 1000 samples, resulting in 20,000 post-burn-in draws in total. A target acceptance rate of 0.95 was used. The convergence of each MCMC run was assessed using various standard diagnostics. First, the rank-normalized split R was required to be less than 1.01, and the effective sample size (*ESS*) to be greater than 100 × number of chains for all parameters. These diagnostics were visualized in Figure S-2. Second, the posterior distributions were

Table 2
Input parameter perturbations used across all global sensitivity analyses. The magnitudes are derived from literature and applied to each nominal parameter set of the corresponding analysis. Each perturbation mimics the effect of a clinical treatment.

Parameter	Perturbation	Reference
Systolic elastance of the left ventricle *Emaxlv*	±20 %	[56,57]
Resistance of the systemic microcirculation *Rmc*	±0.2 mmHg s mL^{-1}	[58,59]
Change in total blood volume *TBV*	±140 mL	[60]

examined alongside trace and rank plots, as shown in Figure S-3. The trace plots for each chain must demonstrate random fluctuations around a stable horizontal band, and all chains need to overlap well to indicate sufficient mixing. Furthermore, it is necessary that the samples span the entire range and do not get stuck at specific values. For the rank plots, the distribution of ranks must be uniform across chains. This is true when all rank bins have approximately the same height, meaning all chains are exploring the same distribution equally. Lastly, autocorrelation is quantified and visualized in Fig. S–4 and was required to decay rapidly toward zero.

In total, four different scenarios were investigated using MCMC, as illustrated in Fig. 2, to address questions relevant to clinical translation:

1. Can MCMC produce parameter posteriors that distinguish different patient conditions?
2. How can sequential updating using prior clinical knowledge and patient trajectories improve parameter posteriors, and how does it compare with MCMC which is performed using uninformative priors?
3. Does sequential updating make predictions of posterior distributions more robust? How do the amount of available measurement data and the intervals of sequential recalibration affect the uncertainties in the posteriors?

More information on the patient's condition, the prior distributions used, and the labels for each scenario can be found in Table 3. Corner plots were used to illustrate the joint parameter distributions of *Emaxlv* and *Rmc* across all four scenarios.

To investigate whether MCMC can identify different patient conditions, patients under normotension and hypotension, both with and without blood loss, were examined. In the first scenario, the patient had normal arterial pressures and cardiac output, and the measurements used for this normotensive scenario (Normo) were derived from synthetic data points. To generate these synthetic data, the following nominal values were specified: CO = [5.0, 5.5, 6.0] L min^{-1}, MAP = [87, 90, 93] mmHg, PP = [39, 40, 41] mmHg, and bpm = [65, 70, 75] min^{-1}. Around each nominal value, normal distributions were created with standard deviations taken from the measurement uncertainties listed in Table 4. From these distributions, 100 samples were drawn, randomly shuffled and concatenated. This resulted in a large sample of synthetic clinical data for each clinical marker, avoiding cross-marker pairing. Six samples were randomly selected from this synthetic data for further analysis, reflecting the limited availability (sparsity) of routine clinical measurements. These samples are listed in Table 5 and were used for the MCMC analysis. To account for measurement uncertainty, the standard deviation of the measurement error for flows and pressures was taken from Table 4. For the remaining scenarios, it was assumed that the patient's blood pressure and cardiac output were dropping and would eventually reach the critical state of hypotension (Hypo), with a MAP of 65 mmHg and a CO of 3 L min^{-1}. In the Hypo A scenario, it was assumed that there was no significant blood volume depletion. In contrast, scenario Hypo B mimics a state of hypotension combined with a mild form of hypovolemia resulting from a blood loss of 333 mL, which corresponds to 61 % of the total stressed blood volume of the healthy baseline. Independent uniform prior distributions were used for the scenario of normotension (Normo) and Hypo A Independent with the bounds listed in Table 1, reflecting the absence of prior clinical knowledge. In contrast, Hypo A and Hypo B Sequential used the posterior from the normotensive scenario as the initial prior, and then

Table 3
General information about the priors and labels used for the different scenarios investigated using parameter inference with MCMC. A graphical visualization can be found in Fig. 2.

Clinical scenario	Prior knowledge	Prior distribution	Scenario label
Normotension	No	Uniform	Normo
Hypotension	No	Uniform	Hypo A Independent
Hypotension	Yes	Posterior from Normo	Hypo A Sequential
Hypotension	Yes	Posterior from Normo	Hypo B Sequential

Table 4
List of measurement uncertainties applied to the observed data used in the MCMC method.

Observation	Uncertainty	Reference
Pressures in mmHg	0.025 × median(pressures) + 2	[64,65]
Flows in L min^{-1}	0.05 × median(flows) + 0.2	[66,67]

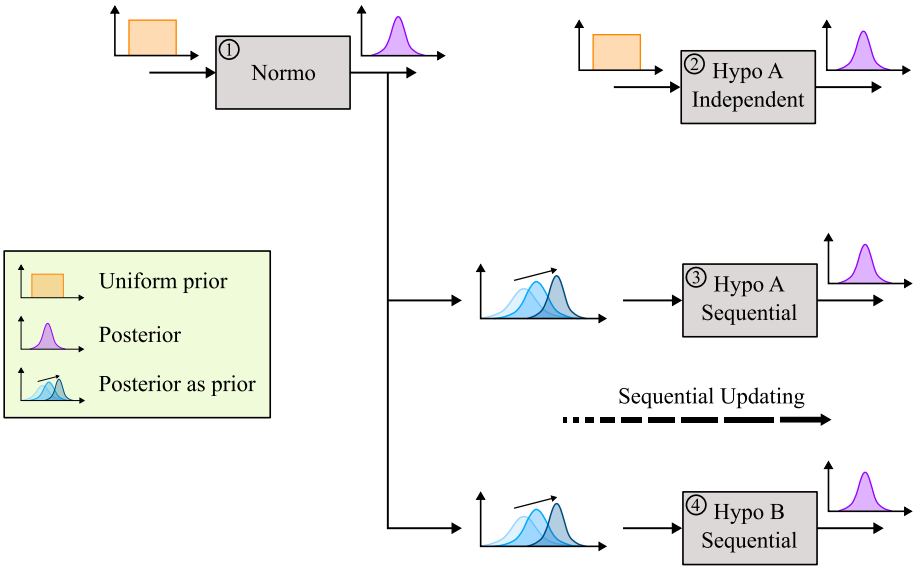

Fig. 2. Overview of the different scenarios investigated using parameter inference with MCMC: (1) Normo and (2) Hypo A Independent are calibrated using uniform priors. (3) Hypo A and (4) Hypo B Sequential use the posteriors from (1) Normo as their initial priors. Then, they iteratively use the posterior from the previous step as the next prior.

Table 5
Measurement data from the different scenarios investigated using parameter inference with MCMC.

Scenario label	*CO* in L min^{-1}	*MAP* in mmHg	*PP* in mmHg	*TBV* in mL	*Bpm* in min^{-1}
Normo	5.8, 5.3, 4.8, 6.3, 6.0, 5.8	89.1, 80.7, 93.9, 96.0, 91.8, 97.1	38.2, 37.1, 37.3, 39.4, 43.9, 47.8	0	66.7, 65.6, 71.1, 71.0, 75.1, 72.9
Hypo A Independent	3.0	65.0	30.0	0	70.0
Hypo A Sequential	3.0	65.0	30.0	0	70.0
Hypo B Sequential	3.0	65.0	30.0	−333	70.0

performed ten sequential calibrations. Each sequential updating with MCMC takes the posterior from the previous step as the next prior, while the observations for *CO*, *MAP,* and *PP* decrease linearly from the baseline value of normotension to the hypotension threshold. The main idea with this sequential updating is to approximate the marginal distribution of the last posterior and fit a multivariate normal distribution to capture dependencies. This is then used with its mean and covariance to define the joint prior for the next calibration step. All of the observation data used for the different scenarios is listed in Table 5.

To compare different approaches of applying MCMC, we compare the standard single-run setup with uniform priors (Hypo A Independent) with a Bayesian sequential updating (Hypo A Sequential), using iterative parameter calibration as described above.

To quantify the effect of the number of patient data points on the uncertainty of the estimated parameter distributions, the normotensive scenario (Normo) was run using 3–30 samples drawn from the synthetic dataset introduced earlier. For each case, MCMC was run, and the coefficients of variation (*CV*) were calculated following

$$CV = \frac{\sigma}{\mu} \tag{6}$$

which relates the standard deviation σ to the mean value μ of each model parameter's posterior distribution. Lastly, the influence of sequential parameter calibration on the posterior uncertainty of each model parameter was quantified by varying the number of calibration steps between normotension to hypotension from 0 to 75 in Hypo A Sequential. *CV* was plotted for the posteriors of each model parameter.

2.4. Sensitivity analysis for classical optimization and Bayesian inference

Sensitivity indices derived from the distributions of the Bayesian inference using MCMC were compared to sensitivities computed from the range of possible local solutions of a classical optimization approach. For that purpose, 1000 samples were drawn from the parameter distributions estimated in Hypo A Sequential, which characterizes hypotension without blood loss. A GSA was performed for each of the 1000 sample points. The ranges for *Emaxlv*, *Rmc*, and *TBV* were derived by applying the perturbations listed in Table 2 to the respective nominal parameter values. Using a sample size of 8000 resulted in $N(2D+2) = 64,000$ evaluations of the previously trained ROM. As a result, uncertainties in the estimation of model parameters were projected onto the derived total order sensitivity indices S_T. Using box plots, the resulting distributions of S_T were compared to the sensitivities, which were obtained for the deterministic point estimates of the classical optimization. These point estimates also characterize the scenario of hypotension with *TBV* = 0 mL.

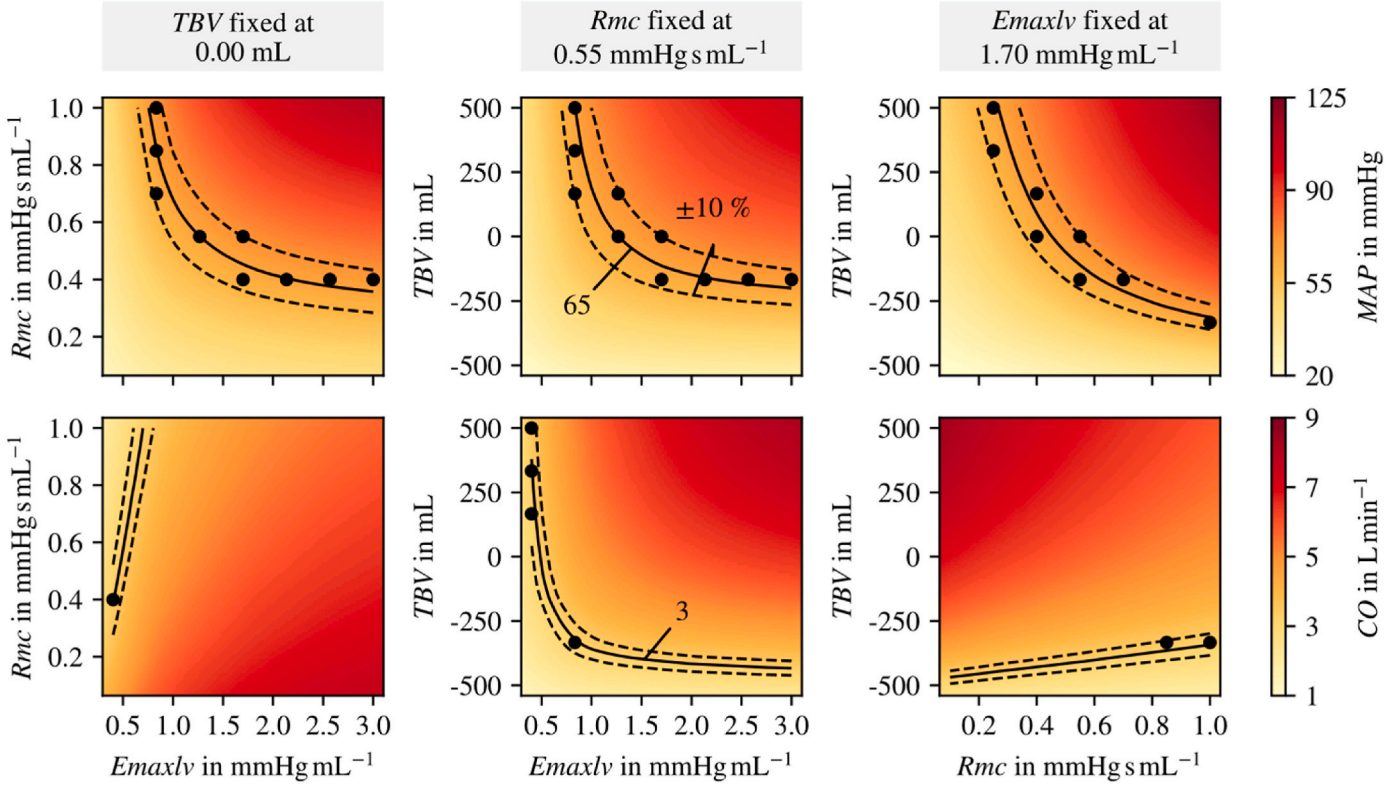

Fig. 3. Mean arterial pressure (*MAP* - first row) and cardiac output (*CO* - second row) for different values of the systolic elastance of the left ventricle *Emaxlv*, the resistance of the systemic microcirculation *Rmc* and the change in total blood volume *TBV*. Candidate point estimates of the parameters that lie within the reference regions of hypotension are displayed as black dots. Columns 1–3 fix the values of *TBV*, *Rmc*, and *Emaxlv* to 0 mL, 0.55 mmHg s mL^{-1}, and 1.7 mmHg mL^{-1}, respectively.

Similarly, distributions of sensitivities were calculated for Hypo B Sequential and compared to the values obtained for Hypo A Sequential. This comparison aims to determine whether these two different patient states influence the magnitude of S_T and its corresponding uncertainty.

3. Results

3.1. Local solutions of classical parameter estimation and implications on sensitivity analysis

Fig. 3 illustrates the issue of non-uniqueness that is often observed in the inverse problem of classical parameter estimation. It shows heatmaps of *MAP* (top row) and *CO* (bottom row) for different values of *Emaxlv*, *Rmc*, and *TBV*. The solid contour line indicates the hypotension reference thresholds of $MAP = 65$ mmHg and $CO = 3$ L min^{-1}, while the dashed contours show ±10 % variation from these thresholds (reference region). The black dots represent candidate point estimates within these regions. Altogether, 28 distinct points were identified within the *MAP* and *CO* reference regions. The reference regions for *MAP* cover the entire range of parameter values. The same applies for the *CO* reference region when *Rmc* is kept constant at 0.55 mmHg s mL^{-1} (second column). However, when *TBV* is fixed at 0 mL (first column), the *CO* reference region is limited to low *Emaxlv* values below 1 mmHg mL^{-1}. With a constant *Emaxlv* of 1.7 mmHg mL^{-1} (third column), a *CO* of 3 L min^{-1} occurs only with blood losses greater than 250 mL. In general, all results for *MAP* and *CO* cover the entire range of physiological values of *Emaxlv*, *Rmc* and *TBV* as reported in the literature. Increasing *Emaxlv*, *Rmc* or *TBV* increases *MAP*, and vice versa. Similarly, a positive correlation exists between *Emaxlv* and *TBV* and *CO*. In contrast, increasing *Rmc* decreases *CO*.

Fig. 4 examines how the parameter non-uniqueness from Fig. 3 translates into model sensitivities with respect to *MAP* and *CO* across the parameter space. It evaluates whether therapy suggestions based on these sensitivities would remain robust across plausible parameter combinations. The figure shows the weighted sum of the total effect S_T of each model parameter, as well as *MAP* (top row) and *CO* (bottom row), for different combinations of parameter values. Blue indicates a high sensitivity of *CO* or *MAP* to *Emaxlv*, magenta to *Rmc*, and yellow to *TBV*. Black dots again mark the samples within the reference region of hypotension. In conditions of hypovolemia with a negative *TBV*, *MAP* is primarily influenced by changes in *TBV*. When *TBV* is positive, however, the influence shifts toward *Rmc*, especially at moderate to low *Rmc*

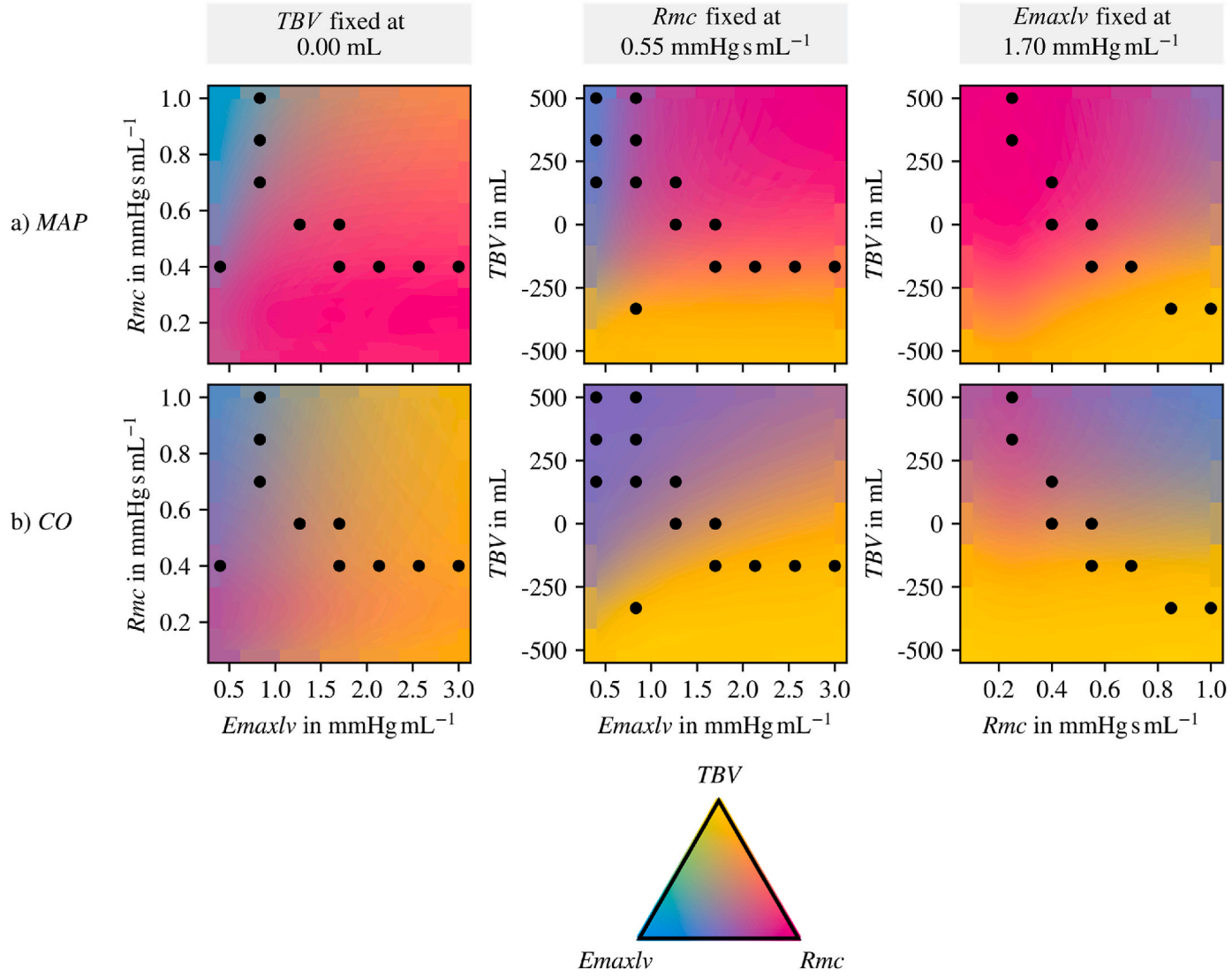

Fig. 4. Weighted sum of the total effect S_T of each model parameter for *MAP* (top row) and *CO* (bottom row). High sensitivity to *Emaxlv* illustrated in blue, to *Rmc* in magenta, and to *TBV* in yellow. Columns 1–3 fix the values of *TBV*, *Rmc*, and *Emaxlv* to 0.00 mL, 0.55 mmHg s mL^{-1}, and 1.70 mmHg mL^{-1}, respectively. (For interpretation of the references to color in this figure legend, the reader is referred to the Web version of this article.)

values. The areas where *Emaxlv* is the most influential parameter are small, i.e., when *Rmc* is high and *Emaxlv* is low. A more balanced influence on *MAP* can be observed when both *Rmc* and *Emaxlv* are high. In this region, *Rmc* and *TBV* are equally sensitive. Conversely, when both *Rmc* and *TBV* are high, *Emaxlv* and *Rmc* dominate changes in *MAP*. *CO* is most affected by changes in *TBV*, especially when *TBV* is negative. Compared to the sensitivities for *MAP*, there are more regions of balanced sensitivity. *Rmc* and *Emaxlv* are only dominant when *TBV* is positive and either *Rmc* is very high or *Emaxlv* is very low. In summary, the contribution of each parameter to the model dynamics is non-unique due to varying parameter sensitivities depending on the chosen parameter combination.

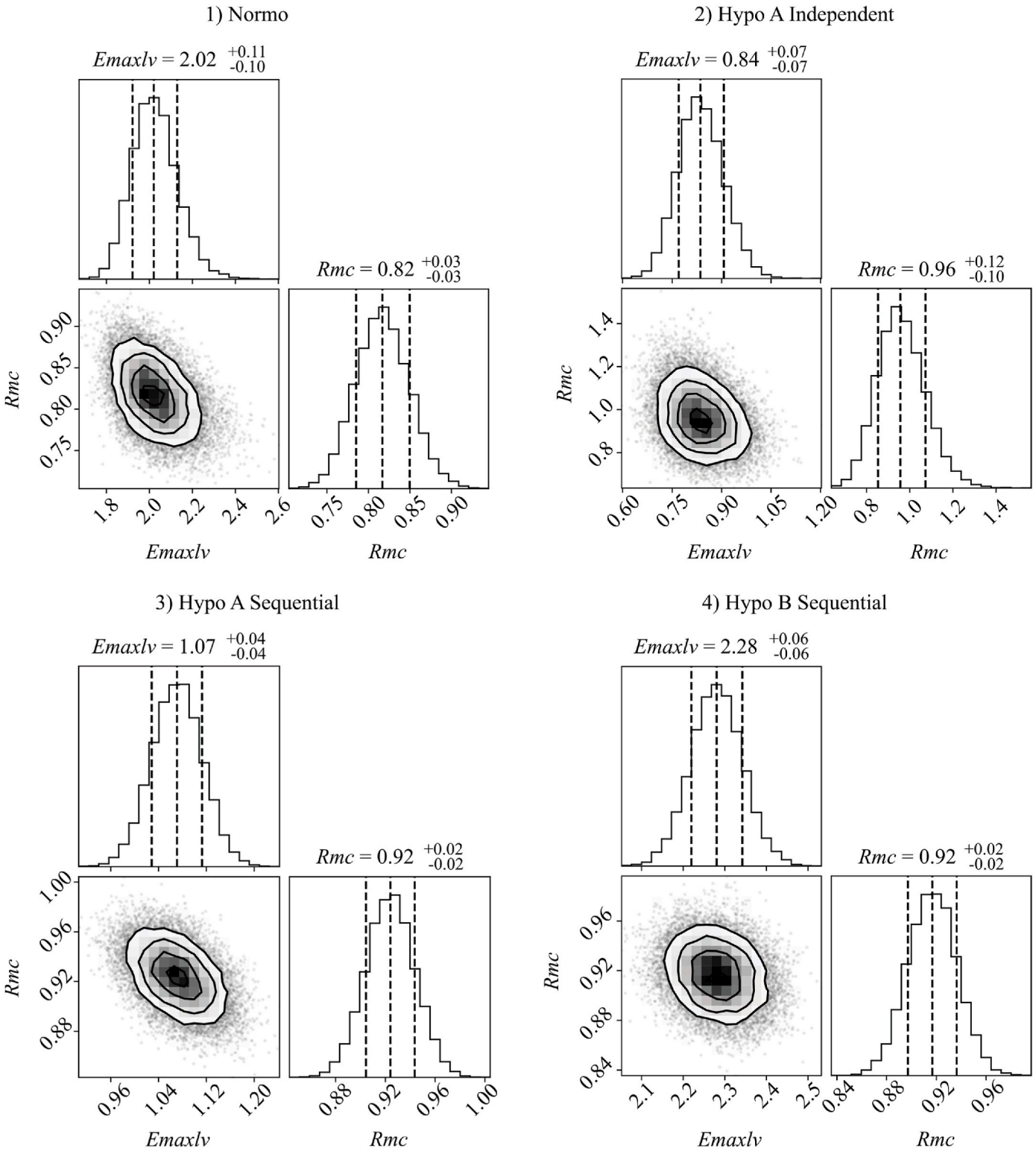

Fig. 5. Corner plots showing posterior distributions of each model parameter for the scenarios 1) Normo, 2) Hypo A Independent, 3) Hypo A Sequential and 4) Hypo B Sequential.

3.2. Parameter estimation using Bayesian approach of MCMC

Fig. 5 examines whether Bayesian inference yields parameter estimates that distinguish between different clinical scenarios. Posterior distributions for *Emaxlv* and *Rmc* are visualized using corner plots and their relationship is visualized by combining scatter and contour plots in a joint posterior density plot. This provides a visualization of potential correlations between the model parameters *Emaxlv* and *Rmc*, thereby allowing an assessment of the practical identifiability of each scenario. Vertical dashed lines mark the 16th, 50th, and 84th percentiles, and the median and standard deviations (68 % credible intervals) are reported above each posterior distribution. Weak to moderate correlations can be observed between the parameters, indicating practical identifiability in all four scenarios. Given normotensive conditions, MCMC estimates the median of *Emaxlv* to be 2.02 mmHg mL^{-1} and *Rmc* to be 0.82 mmHg s mL^{-1}, as can be seen in Fig. 5–1). When the patient suffers from hypotension without any blood loss, displayed in Fig. 5–2), the median of *Emaxlv* decreases to 0.84 mmHg mL^{-1}, and *Rmc* slightly increases to 0.96 mmHg s mL^{-1}, indicating an impaired cardiac function. In contrast, when the prior distributions are informed by the MCMC run for normotension (Hypo A Sequential), the median of *Emaxlv* is slightly higher than in the Hypo A Independent case, with a value of 1.07 mmHg mL^{-1}, and *Rmc* is slightly lower, with a value of 0.92 mmHg s mL^{-1}, as shown in Fig. 5–3). Additionally, the standard deviations decrease in this scenario. For Hypo B Sequential, in which the patient suffers from hypotension combined with a blood loss of 333 mL, the resulting parameter distributions are visualized in Fig. 5–4). The results indicate, that the left ventricular contractility is not impaired, and the median of *Emaxlv* is estimated to be 2.28 mmHg mL^{-1}, with a slight increase of *Rmc* to 0.92 mmHg s mL^{-1}, suggesting the absence of any vasodilation. The evolution of the parameter distributions and their corresponding standard deviations due to a sequential recalibration is illustrated in Figure S-5. The figure shows the posteriors for each intermediate step of a sequential updating with ten steps in total, and compares them with the normotensive condition and Hypo A Independent.

Fig. 6 explores how data availability and the recalibration schedule influence the uncertainty in the inferred parameter posteriors. By quantifying the coefficient of variation across different numbers of data points and sequential recalibration steps, it gives initial directions for clinical implementation. Fig. 6-a) shows the coefficient of variation of the parameter distributions of *Emaxlv* and *Rmc* as a function of the number of clinically measured data points included in the MCMC run for a patient under normotension. The *CV* decreases as more data points are included and exhibits a monotonic, asymptotic behavior. Using 30 data points reduces the uncertainty of the estimated parameter distributions by 70 % and 68 %, respectively, for both *Emaxlv* and *Rmc* compared to the MCMC run with only 3 data points. Across all tested sample sizes, *Emaxlv* remains 17–25 % more uncertain than *Rmc*.

Fig. 6-b) illustrates the coefficient of variation of the parameter distributions of *Emaxlv* and *Rmc* in the final hypotensive state as a function of the number of intermediate steps in the sequential updating performed during the progression of hypotension. As in the previous analysis, a monotonic, asymptotic behavior can be observed, implying that the more calibration steps performed, the lower the coefficient of variation. Here, the magnitudes of uncertainty for both *Emaxlv* and *Rmc* are comparable. Using 75 calibration steps reduces the *CV* for *Emaxlv* and *Rmc* by 85 % and 94 %, respectively. Again, *Emaxlv* is more uncertain than *Rmc*, except for independent calibration without sequential updating.

Figure S-6 and Figure S-7 show the standard deviations and mean values of *Rmc* and *Emaxlv* as a function of 1) the number of patient data points and 2) the number of sequential calibration steps used for MCMC. The standard deviations decrease while the mean values of *Rmc* and *Emaxlv* remain stable, supporting the convergence of the inverse UQ in both cases.

3.3. Uncertainty-aware sensitivity analysis

First, the model's response to perturbations that mimic clinical interventions is quantified using GSA. Sensitivities are derived using multiple plausible solutions of classical optimization as well as Bayesian posterior distributions, depicted in Figure S-8 in the Appendix. Fig. 7 compares the sensitivities from these two approaches in the scenario of hypotension without blood loss. This enables an assessment of the stability of sensitivity rankings and the reliability of therapy recommendations in this setting. It shows box plots of the distributions of the total order sensitivity indices of *Emaxlv*, *Rmc*, and *TBV* for the outputs *CO* and *MAP*. The boxes show the quartiles, and the orange horizontal lines indicate the median sensitivity of each box. The whiskers extend to the most extreme sensitivity values as vertical lines. The solid boxes show the sensitivities for the Bayesian approach Hypo A Sequential. The hatched boxes show the sensitivities from the classical optimization approach, where the deterministic point estimates satisfy $TBV = 0$. The magnitudes of the sensitivity indices S_T and the ranking of the most influential parameters vary depending on the approach. For the classical approach, *TBV* has the greatest impact on *CO*, while the effects of *Rmc* and *Emaxlv* are moderate and small, respectively. In contrast, the Bayesian approach identifies *Rmc* as the most influential parameter, with the impact of *TBV* being moderate and that of *Emaxlv* being small. *Rmc* is the most dominant parameter for *MAP* in both approaches. In general, the classical approach tends to predict higher sensitivities for *Rmc* than the Bayesian approach, but their parameter ranking is the same (*Rmc* → *TBV* → *Emaxlv*). The uncertainties of the sensitivity values are significantly higher in the classical approach, resulting in a less

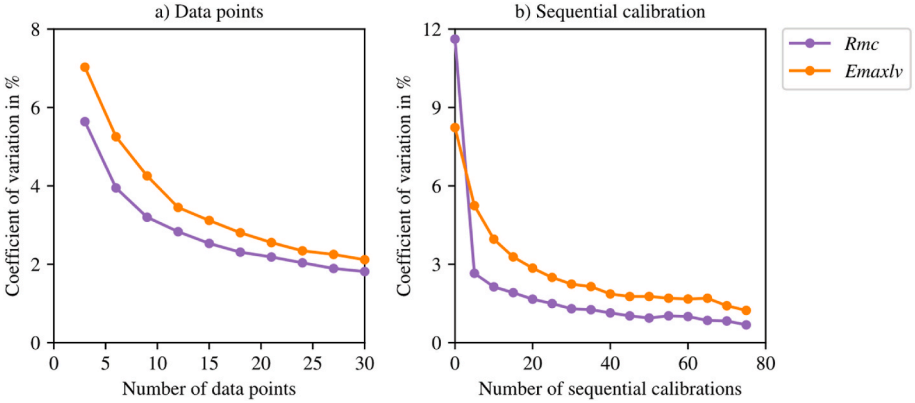

Fig. 6. Coefficient of variation for *Rmc* and *Emaxlv*, depending on a) the number of data points and b) the number of sequential calibration steps included in the parameter inference using MCMC.

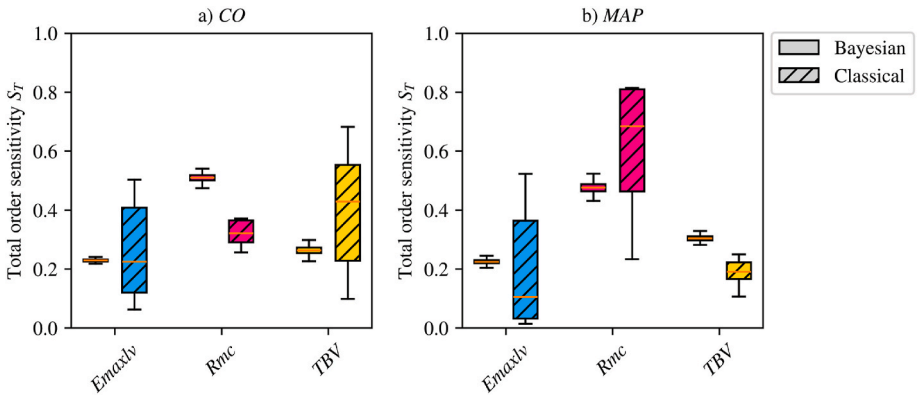

Fig. 7. Distributions of the total order sensitivity indices S_T for each model parameter and output for the Bayesian (Hypo A Sequential) and classical (deterministic point estimates satisfying $TBV = 0$ mL) approaches. Boxes show quartiles, with an orange horizontal line at the median. Whiskers extend to the most extreme sensitivity values. (For interpretation of the references to color in this figure legend, the reader is referred to the Web version of this article.)

stable ranking of the model parameters than in the Bayesian approach.

Lastly, the sensitivity of the model across patient conditions is assessed by running GSAs on posteriors from Hypo A and Hypo B Sequential (hypotension with or without blood loss). This enables a qualitative assessment of the model's predictive capability by comparing derived therapy recommendations with clinical knowledge. For this comparison, Fig. 8 shows the distributions of total order sensitivities S_T, with solid boxes representing Hypo A Sequential and dotted boxes showing Hypo B Sequential. Once again, the boxes depict the quartiles, with an orange line indicating the median sensitivity of each box. The whiskers illustrate the range of values extending to the most extreme sensitivity values. The ranking of the most sensitive model parameters appears to depend on the patient's condition. For Hypo A, both *CO* and *MAP* are mainly affected by *Rmc*, while *Emaxlv* and *TBV* have a comparably moderate impact. In contrast, a reverse ordering of the parameter influence can be seen for Hypo B and *CO*. *Emaxlv* and *TBV* both have a significant impact, while *Rmc* has low S_T values. Changes in *MAP* in scenario Hypo B are mainly driven by *TBV*. The sensitivities in Hypo B appear to show a greater variability than in Hypo A, and these uncertainties are generally greater for *CO* than for *MAP*. Furthermore, the variability is greater for *Emaxlv* and *TBV* than for *Rmc*.

4. Discussion

This study aimed to demonstrate the capability of Bayesian parameter inference using MCMC to find parameter distributions for a 0D cardiovascular model in different clinical scenarios of IOH, as well as highlighting the benefits of integrating prior clinical knowledge and uncertainties. Furthermore, the study aimed to demonstrate how this can be used to introduce an uncertainty-aware sensitivity analysis to support clinical decision-making. We successfully developed a strategy to integrate MCMC into computational models for clinical decision-support. This produced parameter distributions that were both clinically interpretable and meaningful. Combining MCMC with GSA allowed us to propagate uncertainty to model sensitivities, mitigating the issue of non-uniqueness and providing valuable new insights relevant for therapy planning. Four main findings were identified:

1. Non-unique parameter estimates from classical optimization can lead to substantially different model responses to perturbations that mimic clinical interventions.
2. Bayesian parameter inference can identify physiologically meaningful parameter distributions that describe different patient conditions.
3. Posterior uncertainty decreases as more patient data become available and parameters are updated more frequently using sequential calibration.
4. For clinical treatment planning, a GSA based on parameter distributions from inverse UQ provides a better representation of model sensitivity and associated uncertainties than a GSA based on a classical point estimate.

In this work, a ROM was trained using a previously developed cardiovascular LPM and was used to apply MCMC to patients with normo- and hypotension. Different amounts of measurement data and calibration steps were tested to quantify their impact on uncertainties in the predicted parameter distributions. These distributions were used in a sensitivity analysis to quantify the effect of every parameter on the clinical markers within each scenario.

From a technical perspective, with a focus on parameter identifiability and inference, model sensitivity, and uncertainty quantification, the results can be summarized as follows: Fig. 3 illustrates the issue of non-uniqueness of classical optimization approaches for parameter calibration that provide local, point-wise solutions. Even keeping only one of the three parameters fixed resulted in 28 possible solutions for the remaining two free parameters. Consequently, keeping all three parameters free will most likely result in even more possible solutions, further worsening the problem of non-uniqueness. Fig. 4 reveals that applying perturbations (that mimic clinical interventions) to different parameter values that lead to the same values of *MAP* and *CO* leads to a fundamentally different response of the model. This can have significant implications for interpreting the results of a GSA. As outlined in the introduction, GSA outputs are often used to reduce the number of free parameters included in a calibration to experimental or clinical data. Since overall sensitivities differ greatly depending on the chosen nominal values to which perturbations are applied, this affects decisions about which parameters to select for calibration tasks. In addition, for models that account for both individual patient states and patient trajectories (clinical data acquired over the course of therapy), identifying an "incorrect" parameter set at the beginning of the trajectory invalidates subsequent model predictions. It is worth noting that the model is rather simple, with only three parameters calibrated to two measurements (*MAP* and *CO*). Other models, e.g., those from Colunga et al. [33] or Karamolegkos et al. [68], contain more variable parameters, making the issue of non-uniqueness higher dimensional. When using computational models to support clinical decisions, sensitivities that are representative of the wrong patient condition could result in incorrect treatment recommendations.

These problems motivate the use of Bayesian approaches, which can account for uncertainties in estimated sensitivity values. Fig. 7 demonstrates the improvement of combining MCMC with GSA over a GSA based on the range of possible local solutions of a classical optimization. Relying on a single-point estimate from a classical optimization (one point in Fig. 3 that lies within the hypotension reference region) poses

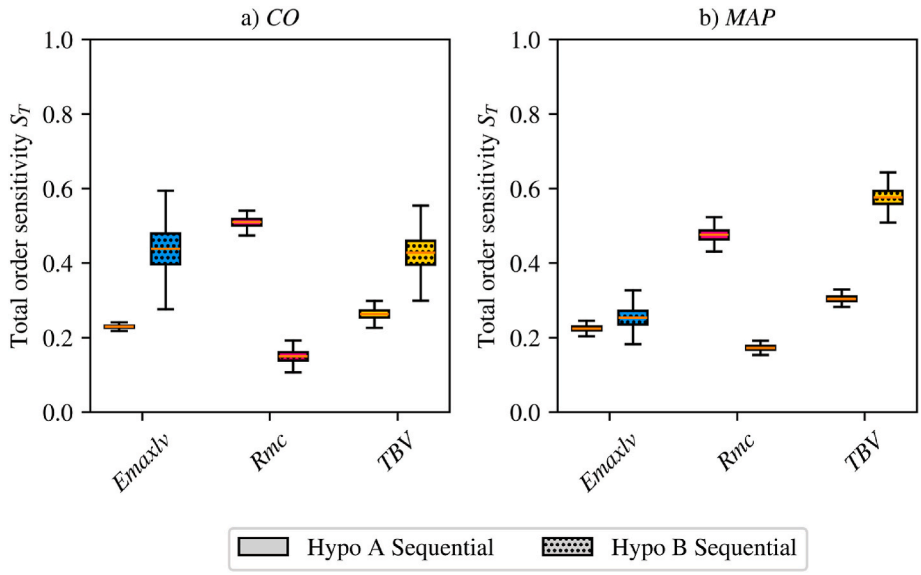

Fig. 8. Distributions of the total order sensitivity indices S_T for each model parameter and output for the Bayesian approaches Hypo A and Hypo B that use sequential calibration. Boxes show quartiles, with an orange horizontal line at the median. Whiskers extend to the most extreme sensitivity values. (For interpretation of the references to color in this figure legend, the reader is referred to the Web version of this article.)

the risk of a model representation that does not accurately reflect the patient. Therefore, the derived sensitivities may provide misleading therapy suggestions. A brute-force strategy (classical optimization from many starting points to collect many possible local solutions), as illustrated in Figs. 3 and 7, still yields unreliable sensitivities that are unsuitable for clinical decision-making. In contrast, combining MCMC and GSA enables one to propagate posterior means and credible intervals onto sensitivity indices, thereby introducing uncertainty quantification of model sensitivity. This information is incredibly valuable for clinicians to judge the reliability of model predictions. Taking this a step further, Fig. 8 shows that this approach works across different patient states and suggests varying treatment modalities accordingly.

This study investigates two methods for integrating Bayesian parameter inference and global sensitivity analysis. First, the independent MCMC approach specifies uninformative uniform prior distributions, giving the sampler the greatest flexibility in finding parameter distributions without introducing excessive expert knowledge. While this simplifies the setup, it may impede the convergence of the MCMC chains to the true posterior distributions, as Argus et al. have outlined [26]. This issue is particularly problematic for complex Bayesian models and small sample sizes, as Lambert et al. have demonstrated [69]. The second approach applies sequential Bayesian updating to incorporate new patient data into parameter posteriors. It uses the parameter distributions from the previous MCMC run as priors for the current iteration. This on-line calibration considers the patient trajectory, which reduces uncertainty in the predicted parameter distributions, as shown in Fig. 6-b). However, introducing clinical knowledge in the priors may bias the sampler and hinder it from exploring the entire possible parameter space between each MCMC run. Nevertheless, this approach is more efficient than a full recalibration, particularly for large datasets, and it has been demonstrated to converge with fewer iterations by DeYoreo et al. [31]. In practice, the choice of priors should depend on the clinical context. For a newly admitted patient, as much data as possible should be collected first. Then, an MCMC with uninformative uniform priors should be performed to obtain a baseline representation of the patient. As new measurement data becomes available over time, the posteriors should be updated using sequential Bayesian updating.

Fig. 5 shows that all posteriors have only weak to moderate correlations between the parameters which indicates good practical identifiability given the respective measurement data and model structure. The scenarios Normo and Hypo A Independent, which use uninformative uniform priors, have slightly broader posterior distributions than the cases that use sequential updating. For *Emaxlv* in Normo and for *Emaxlv* and *Rmc* in Hypo A Independent, the histograms show flat regions on the right tail of the posterior distributions, though with very low probability. This could generally indicate a slightly poorer practical identifiability. In contrast, the posteriors for Hypo A Sequential decay to zero at both tails. This highlights the benefits of sequential updating, which incorporates clinical information into the prior distributions of each calibration step. This study could show how practical identifiability can be improved in different ways. On the one hand, more data helps, as shown in Fig. 6-a). Fig. 6-b) illustrates that a more frequent collection of measurement data and consequently a more frequent recalibration of the model parameters can also be beneficial. Including additional clinical markers, such as central venous pressure, can improve understanding the physiological causes of changes observed in current measurement data.

Interpreting the results with respect to the clinical case of intraoperative hypotension, we observe the following: Using a Bayesian approach with MCMC, parameter distributions for different patient conditions were estimated, identifying the different mechanics that cause a drop in *MAP* and *CO*. In the baseline scenario of normotension, the estimated *Emaxlv* is representative of normal cardiac function [15], and *Rmc* is within the physiological range for the systemic vascular resistance (SVR) [70]. For the Hypo A Sequential scenario (no blood loss and iterative calibration of distributions), the derived parameter distributions suggest an impaired left ventricular contractility, as indicated by a 58 % drop in *Emaxlv* and a 17 % increase in SVR from baseline. These observations are consistent with the proposed parameter values of Shi et al. [71] and the described mechanisms of Wijnberge et al. [4]. In contrast, Hypo B Sequential correctly suggests hypovolemia and preserved cardiac function. These results demonstrate that changes in parameter values identified through MCMC align with clinical observations. This highlights the strength of mechanistic models with physiologically interpretable parameters. Furthermore, integrating a GSA based on parameter distributions obtained by MCMC into clinical practice appears feasible. Ideally, parameters are calibrated once using all available data (Normo) and then updated as new patient data becomes available (Hypo A Sequential). This approach enables continual learning of the model by retaining information from earlier, potentially

non-pathophysiological states. For IOH, this could support the use of more targeted combinations of vasopressors, inotropes, and fluids, which could help reduce the risk of postoperative acute kidney injury [7] or gastrointestinal anastomotic leak [72].

Given that the contractility *Emaxlv* is significantly reduced and *Rmc* is slightly increased for Hypo A Sequential, a balanced treatment approach with inotropes and vasopressors is likely an effective therapy option for this scenario. However, a systematic, variance-based GSA reveals that the treatment with vasopressors is the most efficient way to elevate *MAP* to normal values. Combining both insights may help decide on a therapy that treats the underlying cause and keeps *MAP* within the normal physiological range, as recommended by Saugel et al. [73]. For Hypo B Sequential, the distributions of S_T suggest a more balanced approach of combining low doses of inotropes with the administration of fluid boluses.

Assuming that the change in total blood volume *TBV*, which represents blood loss in the case of hypovolemia, is known exactly (i.e., it is not a free parameter in the calibration), has certain implications for clinical application. It reduces model complexity and enhances parameter identifiability, improving the performance and efficiency of the Bayesian parameter inference. However, Saugel et al. emphasize that quantifying intraoperative blood loss is often challenging [73]. For this reason, a precise approximation of the patient's preoperative blood volume is essential, along with the continuous monitoring of the intraoperative blood loss using one of the methods described by Lin et al. which should be tailored to the specific clinical scenario encountered [74]. In this regard, the observed blood loss and its associated measurement uncertainties should be incorporated into the Bayesian parameter inference. Additionally, sequential updating could account for changes in blood loss or fluid bolus administration over time, ensuring that the posterior distributions reflect the trajectory of the patient's state.

This study has several limitations. First, the Bayesian parameter inference using MCMC was applied to synthetically generated clinical data. This data was created by assuming random Gaussian noise, representing measurement uncertainties, and applying random, independent shuffling. Consequently, the data does not contain physiological dependencies between samples or clinical markers, and it covers only a small range of possible patient states. In the future, to allow direct validation of the derived parameter posteriors, the observed data could be generated using the initial LPM to provide a ground truth for comparison. However, the goal of this study was to demonstrate a methodological proof of concept and there is no reason to assume that real-world clinical data will change the general observations made. The next logical step is applying it to real patient data. Furthermore, the defined measurement uncertainties are based on data sheets of sensors found in the literature. For real clinical applications, these uncertainties must be specific to the sensors and workflows used. Additionally, a ROM based on a relatively simple 0D cardiovascular computational model was used with MCMC to infer model parameter distributions. It consists only of a combination of resistances, compliances, and inertances. It does not include autoregulation, heart-lung interaction, or other complex physiological mechanisms. In addition, the model has not yet been validated for the specific clinical case of IOH. The sensitivity of the model derived from GSA was only compared with general clinical observations. Therefore, it remains to be shown whether the model can make predictions for real, patient-specific conditions. Although models simplify reality, we believe they could serve as future clinical decision-support tools as long as their uncertainty is rigorously assessed using MCMC and sensitivity analysis.

5. Conclusion

Characterizing the behavior of computational physiology models by combining Bayesian inference based on MCMC with sensitivity analysis and incorporating clinical uncertainties can enhance their clinical utility. Our novel approach enables a) determining parameter distributions that reflect different patient states, b) reducing uncertainty in these distributions through sequential updating, and c) performing uncertainty-aware sensitivity analysis with the potential to inform therapy planning. This approach reveals substantial differences in model sensitivity and derived treatment suggestions across patient conditions. Additionally, the uncertainty in sensitivity estimates is significantly reduced compared to approaches based on classical optimization-based point estimation.

CRediT authorship contribution statement

Jan-Niklas Thiel: Writing – original draft, Visualization, Validation, Software, Methodology, Investigation, Funding acquisition, Formal analysis, Data curation, Conceptualization. **Marko Zlicar:** Writing – review & editing, Methodology, Conceptualization. **Ulrich Steinseifer:** Writing – review & editing, Supervision, Resources, Project administration, Funding acquisition. **Borut Kirn:** Writing – review & editing, Resources, Project administration, Methodology, Conceptualization. **Michael Neidlin:** Writing – review & editing, Supervision, Project administration, Methodology, Funding acquisition, Conceptualization.

Ethic statement

This study does not use any clinical data and is based purely on synthetically generated data that is representative of the clinical case of intraoperative hypotension.

Funding

Funded by the Deutsche Forschungsgemeinschaft (DFG, German Research Foundation) SPP2014 "Towards the Artificial Lung" (project number: 447746988) and "Young Investigator Grant" as part of SPP2014.

Declaration of competing interest

The authors declare that they have no known competing financial interests or personal relationships that could have appeared to influence the work reported in this paper.

Appendix A. Supplementary data

Supplementary data to this article can be found online at https://doi.org/10.1016/j.compbiomed.2025.111371.

Data availability

The basic version of the cardiovascular model can be found at the GitHub link https://github.com/nikithiel/ECLIPSE (without implementation of fluid bolus). The code to perform surrogate model training and testing can be accessed through https://github.com/nikithiel/SASQUATCH.

References

[1] F. Guarracino, P. Bertini, Perioperative hypotension: causes and remedies, J. Anesth. Analg. Crit. Care 2 (2022) 17, https://doi.org/10.1186/s44158-022-00045-8.
[2] K. Kouz, P. Hoppe, L. Briesenick, B. Saugel, Intraoperative hypotension: pathophysiology, clinical relevance, and therapeutic approaches, Indian J. Anaesth. 64 (2020) 90–96, https://doi.org/10.4103/ija.IJA_939_19.
[3] F. Hatib, Z. Jian, S. Buddi, C. Lee, J. Settels, K. Sibert, et al., Machine-Learning Algorithm to Predict Hypotension Based on high-fidelity Arterial Pressure Waveform Analysis, 2018, https://doi.org/10.1097/aln.0000000000002300.
[4] M. Wijnberge, B.F. Geerts, L. Hol, N. Lemmers, M.P. Mulder, P. Berge, et al., Effect of a machine learning-derived early warning system for intraoperative hypotension vs standard care on depth and duration of intraoperative hypotension during

elective noncardiac surgery: the HYPE randomized clinical trial, JAMA 323 (2020) 1052–1060, https://doi.org/10.1001/jama.2020.0592.
[5] E. Schneck, D. Schulte, L. Habig, S. Ruhrmann, F. Edinger, M. Markmann, et al., Hypotension prediction index based protocolized haemodynamic management reduces the incidence and duration of intraoperative hypotension in primary total hip arthroplasty: a single centre feasibility randomised blinded prospective interventional trial, J. Clin. Monit. Comput. 34 (2020) 1149–1158, https://doi.org/10.1007/s10877-019-00433-6.
[6] S.J. Davies, S.T. Vistisen, Z. Jian, F. Hatib, T.W.L. Scheeren, Ability of an arterial waveform analysis-derived hypotension prediction index to predict future hypotensive events in surgical patients, Anesth. Analg. 130 (2019) 352–359, https://doi.org/10.1213/ANE.0000000000004121.
[7] C. Chiu, N. Fong, D. Lazzareschi, O. Mavrothalassitis, R. Kothari, L.-L. Chen, et al., Fluids, vasopressors, and acute kidney injury after major abdominal surgery between 2015 and 2019: a multicentre retrospective analysis, Br. J. Anaesth. 129 (2022) 317–326, https://doi.org/10.1016/j.bja.2022.05.002.
[8] D.I. Sessler, J.A. Bloomstone, S. Aronson, C. Berry, T.J. Gan, J.A. Kellum, et al., Perioperative quality initiative consensus statement on intraoperative blood pressure, risk and outcomes for elective surgery, Br. J. Anaesth. 122 (2019) 563–574, https://doi.org/10.1016/j.bja.2019.01.013.
[9] T. Kappen, W.S. Beattie, Perioperative hypotension 2021: a contrarian view, Br. J. Anaesth. 127 (2021) 167–170, https://doi.org/10.1016/j.bja.2021.03.015.
[10] P.S. Myles, R. Bellomo, T. Corcoran, A. Forbes, P. Peyton, D. Story, et al., Restrictive versus liberal fluid therapy for major abdominal surgery, N. Engl. J. Med. 378 (2018) 2263–2274, https://doi.org/10.1056/NEJMoa1801601.
[11] M.J. Scott, Perioperative patients with hemodynamic instability: consensus recommendations of the anesthesia patient safety foundation, Anesth. Analg. 138 (2024) 713–724, https://doi.org/10.1213/ANE.0000000000006789.
[12] M.P. Mulder, M. Harmannij-Markusse, L. Fresiello, D.W. Donker, J.-W. Potters, Hypotension prediction index is equally effective in predicting intraoperative hypotension during noncardiac surgery compared to a mean arterial pressure threshold: a prospective observational study, Anesthesiology 141 (2024) 453–462, https://doi.org/10.1097/ALN.0000000000004990.
[13] J.G. Chase, J.-C. Preiser, J.L. Dickson, A. Pironet, Y.S. Chiew, C.G. Pretty, et al., Next-generation, personalised, model-based critical care medicine: a state-of-the art review of in silico virtual patient models, methods, and cohorts, and how to validation them, Biomed. Eng. Online 17 (2018) 24, https://doi.org/10.1186/s12938-018-0455-y.
[14] T. Arts, T. Delhaas, P. Bovendeerd, X. Verbeek, F.W. Prinzen, Adaptation to mechanical load determines shape and properties of heart and circulation: the CircAdapt model, Am. J. Physiol. Heart Circ. Physiol. 288 (2005) H1943–H1954, https://doi.org/10.1152/ajpheart.00444.2004.
[15] T. Korakianitis, Y. Shi, Numerical simulation of cardiovascular dynamics with healthy and diseased heart valves, J. Biomech. 39 (2006) 1964–1982, https://doi.org/10.1016/j.jbiomech.2005.06.016.
[16] M. Broomé, Elira Maksuti, Anna Bjllmark, Bjrn Frenckner, Birgitta Janerot-Sjberg, Closed-loop real-time simulation model of hemodynamics and oxygen transport in the cardiovascular system, Biomed. Eng. Online (2013), https://doi.org/10.1186/1475-925X-12-69.
[17] A. Quarteroni, A. Veneziani, C. Vergara, Geometric multiscale modeling of the cardiovascular system, between theory and practice, Comput. Methods Appl. Mech. Eng. 302 (2016) 193–252, https://doi.org/10.1016/j.cma.2016.01.007.
[18] A. Pironet, P.C. Dauby, J.G. Chase, P.D. Docherty, J.A. Revie, T. Desaive, Structural identifiability analysis of a cardiovascular system model, Med. Eng. Phys. 38 (2016) 433–441, https://doi.org/10.1016/j.medengphy.2016.02.005.
[19] H. Miao, X. Xia, A.S. Perelson, H. Wu, On identifiability of nonlinear ODE models and applications in viral dynamics, SIAM Rev. Soc. Ind. Appl. Math. 53 (2011) 3–39, https://doi.org/10.1137/090757009.
[20] A. Raue, C. Kreutz, T. Maiwald, J. Bachmann, M. Schilling, U. Klingmüller, J. Timmer, Structural and practical identifiability analysis of partially observed dynamical models by exploiting the profile likelihood, Bioinformatics 25 (2009) 1923–1929, https://doi.org/10.1093/bioinformatics/btp358.
[21] M. Salvador, F. Regazzoni, L. Dede, A. Quarteroni, Fast and robust parameter estimation with uncertainty quantification for the cardiac function, Comput. Methods Progr. Biomed. 231 (2023) 107402, https://doi.org/10.1016/j.cmpb.2023.107402.
[22] A. Tonini, F. Regazzoni, M. Salvador, L. Dede, R. Scrofani, L. Fusini, et al., Two new calibration techniques of lumped-parameter mathematical models for the cardiovascular system, Num. Meth Eng. (2025), https://doi.org/10.1002/nme.7648.
[23] N.L. Bjørdalsbakke, J.T. Sturdy, D.R. Hose, L.R. Hellevik, Parameter estimation for closed-loop lumped parameter models of the systemic circulation using synthetic data, Math. Biosci. 343 (2022) 108731, https://doi.org/10.1016/j.mbs.2021.108731.
[24] R. Laubscher, J. van der Merwe, P. Herbst, J. Liebenberg, Estimation of simulated left ventricle elastance using lumped parameter modelling and gradient-based optimization with forward-mode automatic differentiation based on synthetically generated noninvasive data, J. Biomech. Eng. (2023), https://doi.org/10.1115/1.4055565.
[25] C.H. Olsen, J.T. Ottesen, R.C. Smith, M.S. Olufsen, Parameter subset selection techniques for problems in mathematical biology, Biol. Cybern. 113 (2019) 121–138, https://doi.org/10.1007/s00422-018-0784-8.
[26] F. Argus, D. Zhao, T.P. Babarenda Gamage, M.P. Nash, G.D. Maso Talou, Automated model calibration with parallel MCMC: applications for a cardiovascular system model, Front. Physiol. 13 (2022) 1018134, https://doi.org/10.3389/fphys.2022.1018134.
[27] J.S. Speagle, A conceptual introduction to Markov chain Monte Carlo methods, arXiv (2020), https://doi.org/10.48550/arXiv.1909.12313.
[28] S. Särkkä, L. Svensson, Bayesian Filtering and Smoothing, Cambridge University Press, New York, 2023.
[29] M.B. Hooten, D.S. Johnson, B.M. Brost, Making recursive bayesian inference accessible, Am. Statistician 75 (2021) 185–194, https://doi.org/10.1080/00031305.2019.1665584.
[30] P. Agand, M. Chen, H.D. Taghirad, Online probabilistic model identification using adaptive recursive MCMC, 2023 Int. Joint Conf. Neural Netw. (2023) 1–8, https://doi.org/10.1109/IJCNN54540.2023.10191118, 18.06.2023 - 23.06.2023; Gold Coast, Australia: IEEE.
[31] M. DeYoreo, C.M. Rutter, J. Ozik, N. Collier, Sequentially calibrating a Bayesian microsimulation model to incorporate new information and assumptions, BMC Med. Inf. Decis. Making 22 (2022) 12, https://doi.org/10.1186/s12911-021-01726-0.
[32] J. Kirkpatrick, R. Pascanu, N. Rabinowitz, J. Veness, G. Desjardins, A.A. Rusu, et al., Overcoming catastrophic forgetting in neural networks, Proc. Natl. Acad. Sci. USA 114 (2017) 3521–3526, https://doi.org/10.1073/pnas.1611835114.
[33] A.L. Colunga, K.G. Kim, N.P. Woodall, T.F. Dardas, J.H. Gennari, M.S. Olufsen, B. E. Carlson, Deep phenotyping of cardiac function in heart transplant patients using cardiovascular system models, J. Physiol. 598 (2020) 3203–3222, https://doi.org/10.1113/JP279393.
[34] D.E. Schiavazzi, A. Baretta, G. Pennati, T.-Y. Hsia, A.L. Marsden, Patient-specific parameter estimation in single-ventricle lumped circulation models under uncertainty, Int. J. Numer. Methods Biomed. Eng. (2017), https://doi.org/10.1002/cnm.2799.
[35] J. Richter, J. Nitzler, L. Pegolotti, K. Menon, J. Biehler, W.A. Wall, et al., Bayesian Windkessel calibration using optimized zero-dimensional surrogate models, Philos. Trans. A Math. Phys. Eng. Sci. 383 (2025) 20240223, https://doi.org/10.1098/rsta.2024.0223.
[36] K. Menon, A. Zanoni, M.O. Khan, G. Geraci, K. Nieman, D.E. Schiavazzi, A. L. Marsden, Personalized and uncertainty-aware coronary hemodynamics simulations: from Bayesian estimation to improved multi-fidelity uncertainty quantification, Comput. Methods Progr. Biomed. 271 (2025) 108951, https://doi.org/10.1016/j.cmpb.2025.108951.
[37] M. Salvador, M. Strocchi, F. Regazzoni, C.M. Augustin, L. Dede, S.A. Niederer, A. Quarteroni, Whole-heart electromechanical simulations using latent neural ordinary differential equations, npj Digit. Med. 7 (2024) 90, https://doi.org/10.1038/s41746-024-01084-x.
[38] I.M. Sobol, Global sensitivity indices for nonlinear mathematical models and their Monte Carlo estimates, Math. Comput. Simulat. (2001) 271–280, https://doi.org/10.1016/S0378-4754(00)00270-6.
[39] A. Puy, W. Becker, S. Lo Piano, A. Saltelli, A comprehensive comparison of total-order estimators for global, Int. J. Uncertain. Quantif. 12 (2022) 1–18, https://doi.org/10.1615/Int.J.UncertaintyQuantification.2021038133.
[40] H. Saxton, X. Xu, T. Schenkel, I. Halliday, Assessing input parameter hyperspace and parameter identifiability in a cardiovascular system model via sensitivity analysis, J. Comput. Sci. 79 (2024) 102287, https://doi.org/10.1016/j.jocs.2024.102287.
[41] L.M. Ellwein, H.T. Tran, C. Zapata, V. Novak, M.S. Olufsen, Sensitivity analysis and model assessment: mathematical models for arterial blood flow and blood pressure, Cardiovasc. Eng. 8 (2008) 94–108, https://doi.org/10.1007/s10558-007-9047-3.
[42] V.G. Eck, W.P. Donders, J. Sturdy, J. Feinberg, T. Delhaas, L.R. Hellevik, W. Huberts, A guide to uncertainty quantification and sensitivity analysis for cardiovascular applications, Int. J. Numer. Methods Biomed. Eng. (2016), https://doi.org/10.1002/cnm.2755.
[43] M.S. Olufsen, J.T. Ottesen, A practical approach to parameter estimation applied to model predicting heart rate regulation, J. Math. Biol. 67 (2013) 39–68, https://doi.org/10.1007/s00285-012-0535-8.
[44] E. Karabelas, S. Longobardi, J. Fuchsberger, O. Razeghi, C. Rodero, M. Strocchi, et al., Global sensitivity analysis of four chamber heart hemodynamics using surrogate models, IEEE Trans. Biomed. Eng. 69 (2022) 3216–3223, https://doi.org/10.1109/TBME.2022.3163428.
[45] M. Strocchi, S. Longobardi, C.M. Augustin, M.A.F. Gsell, A. Petras, C.A. Rinaldi, et al., Cell to whole organ global sensitivity analysis on a four-chamber heart electromechanics model using Gaussian processes emulators, PLoS Comput. Biol. 19 (2023) e1011257, https://doi.org/10.1371/journal.pcbi.1011257.
[46] H. Saxton, D.J. Taylor, G. Faulkner, I. Halliday, T. Newman, T. Schenkel, et al., The impact of experimental designs & system sloppiness on the personalisation process: a cardiovascular perspective, PLoS One 20 (2025) e0326112, https://doi.org/10.1371/journal.pone.0326112.
[47] A.L. Colunga, M.J. Colebank, M.S. Olufsen, Parameter inference in a computational model of haemodynamics in pulmonary hypertension, J. R. Soc. Interface 20 (2023) 20220735, https://doi.org/10.1098/rsif.2022.0735.
[48] S. Longobardi, A. Lewalle, S. Coveney, I. Sjaastad, E.K.S. Espe, W.E. Louch, et al., Predicting left ventricular contractile function via Gaussian process emulation in aortic-banded rats, Philos. Trans. A Math. Phys. Eng. Sci. 378 (2020) 20190334, https://doi.org/10.1098/rsta.2019.0334.
[49] O. Eriksson, A. Jauhiainen, Sasane S. Maad, A. Kramer, A.G. Nair, C. Sartorius, J. Hellgren Kotaleski, Uncertainty quantification, propagation and characterization by Bayesian analysis combined with global sensitivity analysis applied to dynamical intracellular pathway models, Bioinformatics 35 (2019) 284–292, https://doi.org/10.1093/bioinformatics/bty607.
[50] K. Tunedal, T. Ebbers, G. Cedersund, Uncertainty in cardiovascular digital twins despite non-normal errors in 4D flow MRI: identifying reliable biomarkers such as

ventricular relaxation rate, Comput. Biol. Med. 188 (2025) 109878, https://doi.org/10.1016/j.compbiomed.2025.109878.
[51] J.M. Hanna, P. Varsos, J. Kowalski, L. Sala, R. Meiburg, I.E. Vignon-Clementel, A comparative analysis of metamodels for 0D cardiovascular models, and pipeline for sensitivity analysis, parameter estimation, and uncertainty quantification, Comput. Biol. Med. 193 (2025) 110381, https://doi.org/10.1016/j.compbiomed.2025.110381.
[52] R.D. Riley, G.S. Collins, L. Kirton, K.I. Snell, J. Ensor, R. Whittle, et al., Uncertainty of risk estimates from clinical prediction models: rationale, challenges, and approaches, BMJ 388 (2025) e080749, https://doi.org/10.1136/bmj-2024-080749.
[53] J.-N. Thiel, A.M. Costa, B. Wiegmann, J. Arens, U. Steinseifer, M. Neidlin, Quantifying the influence of combined lung and kidney support using a cardiovascular model and sensitivity analysis-informed parameter identification, Comput. Biol. Med. 186 (2025) 109668, https://doi.org/10.1016/j.compbiomed.2025.109668.
[54] S. Ceruti, L. Anselmi, B. Minotti, D. Franceschini, J. Aguirre, A. Borgeat, A. Saporito, Prevention of arterial hypotension after spinal anaesthesia using vena cava ultrasound to guide fluid management, Br. J. Anaesth. 120 (2018) 101–108, https://doi.org/10.1016/j.bja.2017.08.001.
[55] J.-N. Thiel, J. Gestrich, U. Steinseifer, I. Friehs, D. Diaz-Gil, M. Neidlin, Quantifying the impact of mitral valve anatomy on clinical markers using surrogate models and sensitivity analysis, Comput. Biol. Med. 192 (2025) 110265, https://doi.org/10.1016/j.compbiomed.2025.110265.
[56] S. Ishizaka, H. Asanoi, T. Kameyama, S. Sasayama, Ventricular-load optimization by inotropic stimulation in patients with heart failure, Int. J. Cardiol. 31 (1990) 51–59.
[57] P.-G. Guinot, D. Longrois, S. Kamel, E. Lorne, H. Dupont, Ventriculo-arterial coupling analysis predicts the hemodynamic response to norepinephrine in hypotensive postoperative patients: a prospective observational study, Crit. Care Med. 46 (2018) e17–e25, https://doi.org/10.1097/CCM.0000000000002772.
[58] R.A. Dyer, A. Daniels, A. Vorster, A. Emmanuel, M.J. Arcache, S. Schulein, et al., Maternal cardiac output response to colloid preload and vasopressor therapy during spinal anaesthesia for caesarean section in patients with severe pre-eclampsia: a randomised, controlled trial, Anaesthesia 73 (2018) 23–31, https://doi.org/10.1111/anae.14040.
[59] D.W. Landry, H.R. Levin, E.M. Gallant, R.C. Ashton, S. Seo, D. D'Alessandro, et al., Vasopressin deficiency contributes to the vasodilation of septic shock, Circulation 95 (1997) 1122–1125, https://doi.org/10.1161/01.cir.95.5.1122.
[60] T.-T. Ni, Z.-F. Zhou, B. He, Q.-H. Zhou, Inferior vena cava collapsibility index can predict hypotension and guide fluid management after spinal anesthesia, Front. Surg. 9 (2022) 831539, https://doi.org/10.3389/fsurg.2022.831539.
[61] K. Cheng, Z. Lu, C. Ling, S. Zhou, Surrogate-assisted global sensitivity analysis: an overview, Struct. Multidiscip. Optim. 61 (2020) 1187–1213, https://doi.org/10.1007/s00158-019-02413-5.
[62] R. van de Schoot, S. Depaoli, R. King, B. Kramer, K. Märtens, M.G. Tadesse, et al., Bayesian statistics and modelling, Nat. Rev. Methods Primers (2021), https://doi.org/10.1038/s43586-020-00001-2.
[63] F. Hartig, J.M. Calabrese, B. Reineking, T. Wiegand, A. Huth, Statistical inference for stochastic simulation models–theory and application, Ecol. Lett. 14 (2011) 816–827, https://doi.org/10.1111/j.1461-0248.2011.01640.x.
[64] Edwards Lifesciences, Edwards TruWave Pressure Monitoring Kit with TrueWave Disposable Pressure Transducer, 2024.
[65] C. Oh, S. Lee, S. Jeon, H. Park, W. Chung, M.-S. Shim, et al., Errors in pressure measurements due to changes in pressure transducer levels during adult cardiac surgery: a prospective observational study, BMC Anesthesiol. 23 (2023) 8, https://doi.org/10.1186/s12871-023-01968-7.
[66] E. Argueta, G. Berdine, C. Pena, K.M. Nugent, FloTrac® monitoring system: what are its uses in critically ill medical patients? Am. J. Med. Sci. 349 (2015) 352–356, https://doi.org/10.1097/MAJ.0000000000000393.
[67] L. Vetrugno, F. Barbariol, C. Deana, Comparison between FlowTrac and Pulmonary Arterial Catheter in Off-Pump Cardiac Surgery Patients: "why Did We Miss Our Appointment?". Comment on Oh et al. Comparison between Fourth-Generation FloTrac/Vigileo System and Continuous Thermodilution Technique for Cardiac Output Estimation after Time Adjustment during Off-Pump Coronary Artery Bypass Graft Surgery: a Retrospective Cohort Study, J. Clin. Med. 11 (2022) 6093, https://doi.org/10.3390/jcm12062343. J Clin Med 2023.
[68] N. Karamolegkos, A. Albanese, N.W. Chbat, Heart-lung interactions during mechanical ventilation: analysis via a cardiopulmonary simulation model, IEEE Open J. Eng. Med. Biol. 2 (2021) 324–341, https://doi.org/10.1109/OJEMB.2021.3128629.
[69] P.C. Lambert, A.J. Sutton, P.R. Burton, K.R. Abrams, D.R. Jones, How vague is vague? A simulation study of the impact of the use of vague prior distributions in MCMC using WinBUGS, Stat. Med. 24 (2005) 2401–2428, https://doi.org/10.1002/sim.2112.
[70] D. Zippes, P. Libby, R. Bonow, E. Braunwald, Heart Disease: a Textbook of Cardiovascular Medicine, seventh ed., Elsevier Science, 2004.
[71] Y. Shi, P.V. Lawford, D.R. Hose, Numerical modeling of hemodynamics with pulsatile impeller pump support, Ann. Biomed. Eng. 38 (2010) 2621–2634, https://doi.org/10.1007/s10439-010-0001-y.
[72] T. Zakrison, B.A. Nascimento, L.N. Tremblay, A. Kiss, S.B. Rizoli, Perioperative vasopressors are associated with an increased risk of gastrointestinal anastomotic leakage, World J. Surg. 31 (2007) 1627–1634, https://doi.org/10.1007/s00268-007-9113-4.
[73] B. Saugel, W. Buhre, M.S. Chew, B. Cholley, M. Coburn, B. Cohen, et al., Intra-operative haemodynamic monitoring and management of adults having noncardiac surgery: a statement from the European society of anaesthesiology and intensive care, Eur. J. Anaesthesiol. 42 (2025) 543–556, https://doi.org/10.1097/EJA.0000000000002174.
[74] Y.-M. Lin, C. Yu, G.-Z. Xian, Calculation methods for intraoperative blood loss: a literature review, BMC Surg. 24 (2024) 394, https://doi.org/10.1186/s12893-024-02699-3.